Kinetics of gallium films confined at grain boundaries

H. Konrad,* J. Weissmüller, and R. Birringer
Universität des Saarlandes, Postfach 15 11 50, 66041 Saarbrücken, Germany

C. Karmonik
National Institute of Standards and Technology, Gaithersburg, Maryland

H. Gleiter
Forschungszentrum Karlsruhe, Postfach 36 40, 76021 Karlsruhe, Germany
(Received 8 September 1997; revised manuscript received 23 March 1998)

We report on a combined study, by *in situ* x-ray diffraction at temperatures between 293 and 80 K, differential scanning calorimetry, and coherent quasielastic neutron scattering (QENS), of thin Ga films confined at grain boundaries in Al_2O_3-Ga nanocomposites that are produced by high-energy ball milling. We find that a molar fraction of Ga of up to 0.18 does not undergo phase change in the temperature interval investigated, which contains the bulk melting temperature T_M^{bulk}, and conclude that this Ga is located in confined layers at grain boundaries, with an estimated thickness of six atomic monolayers. In samples with a higher overall molar fraction, the Ga in excess of molar fraction 0.18 melts and crystallizes reversibly when cycled between 100 and 320 K. For such samples, QENS at 320 K, that is, 17 K above T_M^{bulk}, indicates three distinct diffusion coefficients D for Ga: one below the resolution limit, $D_1 < 1\times10^{-6}$ cm^2/s, one agreeing with the bulk liquid value, $D_2 = 3.4\times10^{-5}$ cm^2/s, and a faster coefficient $D_3 = 2.4\times10^{-4}$ cm^2/s. We argue that the smaller and medium diffusion coefficients, D_1 and D_2, represent, respectively, solidlike layers near the Al_2O_3-Ga interface and liquid Ga in the core of interfacial layers and in liquid droplets. The fast diffusion coefficient (D_3) may be due to diffusion on free surfaces. [S0163-1829(98)06728-9]

I. INTRODUCTION

The last few years have witnessed renewed interest in the properties of liquids confined within very narrow spaces, e.g., in small pores or capillaries or in molecularly thin films adsorbed on substrates or confined between two surfaces. This interest has extended to both the static and dynamic properties of the confined liquids. There exists general agreement that properties of bulk liquids may change substantially by the confinement. Several studies of the melting behavior of materials in confined geometries have been reported. For instance, computer simulations[1–3] as well as experimental data on inert gases in porous glasses,[4] for water and nonpolar organic liquids in intercalates[5] and for Ge/Pb/Ge layers[6] reveal that melting in confined geometries is a broad transition that starts up to 40 K below the bulk melting temperature. A useful tool for studying the premelting of thin adsorbed films is quasielastic neutron scattering.[7,8] This technique allows us not only to investigate the diffusion mechanism of the film atoms but also to determine the temperature dependence of the liquid fraction. Some experiments indicate that even above the melting point ordering (stratification) of the first few monolayers adjacent to the interface persists due to steric forces[9] or compression[10] of these layers or due to chemical bonding.[11] The dynamic properties of ultrathin films between two molecularly smooth surfaces sliding past each other have also been investigated.[12] These studies clearly reveal film properties that are profoundly different from those of bulk liquids. Once the film thickness falls below five molecular diameters, these liquid films exhibit solidlike properties, i.e., support uniaxial stress as well as shear stress.

Recently, a new approach to study thin films in confined geometry was realized by preparing composites of a nanocrystalline (i.e., polycrystalline with a mean grain size of the order of 10 nm) matrix and wetting films in the grain boundaries.[13] These alloys were produced by modifying the standard inert gas condensation process used for preparing single-phase nanocrystalline solids[14] so that isolated nm-sized *W* particles are coated *in situ* with Ga prior to being consolidated into a bulk solid. Thus, it was possible to incorporate several layers of Ga in the grain boundaries of nanocrystalline *W*. Because of their high specific grain boundary area the nanocrystalline microstructure can incorporate large volume fractions (up to 50 vol %) of grain boundary films and thus offer the unique opportunity to investigate thin films at grain boundaries by volume-sensitive methods such as x-ray scattering or neutron scattering. In the present work, we used high-energy ball milling to prepare a similar composite microstructure. The choice of the components, alumina (Al_2O_3) as the matrix and Ga as the film, is motivated by the favorable combination of melting points, that of Ga being close to room temperature (303 K), thus allowing experiments at the film melting point without irreversible changes of the microstructure of the high melting point matrix. Furthermore, alumina has a suitably low electron density compared to Ga so that x-ray scattering cross sections of the composite contain relatively strong contributions from the Ga. High energy ball milling, a method that is being used extensively to prepare nanostructured samples[15] was chosen as the method of preparation, because in contrast to inert gas condensation, it allows for convenient preparation of the

comparatively large quantities of sample required for neutron scattering studies.

Here we report on a combined investigation of the structure and dynamics of alumina-Ga composite nanostructures by *in situ* x-ray diffraction between 293 and 80 K, differential scanning calorimetry, and quasielastic neutron scattering.

II. EXPERIMENTAL PROCEDURE AND DATA ANALYSIS

Nanocomposites of composition $(Al_2O_3)_{(1-x)}Ga_x$, with molar fractions x of Ga in the interval $0 \Leftarrow x \Leftarrow 0.4$ were prepared by high-energy ball milling in a Spex2000 mill. For minimizing contamination by wear from the hardened steal vials, it was found suitable to proceed as follows: first, commercial alumina powder (Pechiney Altech, purity: 99.9%) was milled for 4 h, which refined the grain size to 25 nm. Then Ga (Heraeus, purity: 99.999%) was added and the milling vial heated for 1 h at 100 °C in order to melt the Ga. The sample was then milled for an additional 1-h period, so that a fine dark gray powder was obtained, with a powder particle size in the μm range. The last two steps were omitted for the sample with $x=0$. Contamination by wear was found to be 1 at % Fe (metal atom fraction), as determined by energy-dispersive analysis with a scanning microscope. Fe has negligible solubility in liquid Ga near the Ga melting point, and is thus concluded to have no noticeable influence on the properties of the Ga phase. Of the intermetallic Ga phases, none was detected by x-ray scattering.

The x-ray diffraction patterns were recorded with a Siemens D5000 θ-θ diffractometer equipped with a cooling stage. We used Mo-K$\alpha_{1/2}$ radiation and a Si(Li) detector. The mean grain size was computed from the broadening of the Bragg reflections after correction for microstrain.[16]

Differential scanning calorimetry (DSC) was carried out in a Perkin Elmer DSC7 in the temperature range 100–320 K. Heating cycles were performed for all samples, and a cooling cycle was recorded for the sample with $x=0.3$. In general, three melting peaks occurred upon heating. The total heat of fusion was calculated by integrating the area under each melting peak, and was converted to a molten molar fraction of Ga using literature values for the molar enthalpy of fusion of the respective phases.[17] The sum of the molten amounts of Ga in the temperature interval 100–320 K constitutes the molar fraction of Ga that melts and crystallizes reversibly in the temperature interval 100–320 K, x_{molten}. When all Ga in the sample is found to melt, then $x_{\text{molten}}=x$.

The diffusivity of the Ga was investigated for several temperatures in and near the interval of the melting transitions by means of quasielastic neutron scattering (QENS).[18] The as-prepared sample with $x=0.3$ Ga was first measured at 288 K, then cooled to 77 K and upon heating spectra at 250, 270, 290, 303, and 320 K were recorded. Upon cooling the measurements at 303 and 290 K were repeated. A pure Ga reference sample was measured at 320 K and in the undercooled liquid state at 290 K. Approximately 100 spectra were recorded at the time-of-flight spectrometer IN5 at ILL, Grenoble[19] at scattering angles θ with $11° < 2\theta < 130°$. The wavelength λ of the incoming neutrons was defined by a four chopper system to a value of 3 Å giving an instrumental energy resolution of 506 μeV half-width at half-maximum (HWHM), a symmetric energy transfer of about 5 meV and a maximum Q value of 3.83 Å^{-1}; Q is the scattering vector given by $Q=4\pi \sin\theta/\lambda$. The 200-K data was used to define the instrumental resolution. Multiple scattering was corrected for by applying the program DISCUS.[20] Apart from a negligible incoherent scattering contribution (incoherent scattering cross section $\sigma_{\text{inc}}^{\text{Al}}=0.0092$),[21] the scattered intensity of the crystalline alumina appears only at Bragg angles. For QENS only angles between the Bragg positions of alumina were investigated, hence the intensity of the spectra originates practically exclusively from elastic and quasielastic scattering of solid or liquid Ga.

Since Ga is a purely coherent scatterer ($\sigma_{\text{coh}}^{\text{Ga}}=6.674$),[21] coherent QENS was measured. In the more commonly used technique of *incoherent* (*a*/*o* to coherent) QENS, the HWHM ω of the quasielastic broadened line can be related to the self-diffusion coefficient D_{self} by

$$\hbar^* \omega = D_{\text{self}} Q^2. \tag{1}$$

For alloys, coherent QENS satisfies Eq. (1) with D_{chem}, the chemical diffusion coefficient, substituted for D_{self}. To identify the appropriate diffusion coefficient for the case of coherent QENS by a single component substance, consider the relation between the coherent and incoherent structure factors, $S(\mathbf{Q})$ and $S_{\text{inc}}(\mathbf{Q})$, respectively, and the time-dependent van Hove (total) correlation and self-correlation functions, $G(\mathbf{r},t)$ and $G_{\text{self}}(\mathbf{r},t)$, respectively:[22]

$$S(\mathbf{Q},\omega) = 1/2\pi \int\int G(\mathbf{r},t)\exp(i\mathbf{Q}\mathbf{r})\exp(-i\omega t)d\mathbf{r}\,dt, \tag{2a}$$

$$S_{\text{inc}}(\mathbf{Q},\omega) = 1/2\pi \int\int G_{\text{self}}(\mathbf{r},t)\exp(i\mathbf{Q}\mathbf{r})\exp(-i\omega t)d\mathbf{r}\,dt. \tag{2b}$$

$G_{\text{self}}(\mathbf{r},t)$ denotes the conditional probability that a particle originally located at position $\mathbf{r}=0$ at time $t=0$ is located at position $\mathbf{r}$ at time t. Given the same initial condition, $G(\mathbf{r},t)$ denotes the probability that there is *any* particle located at position $\mathbf{r}$ at time t.

With a Gaussian form of $G_{\text{self}}(\mathbf{r},t)$,

$$G_{\text{self}}(\mathbf{r},t) = (4D_{\text{self}}t)^{-3/2} \exp(-r^2/4D_{\text{self}}t),$$

Eq. (2b) leads to a Lorentzian energy dependence of $S_{\text{inc}}(\mathbf{Q})$,

$$S_{\text{inc}}(\mathbf{Q},\omega) = D_{\text{self}}\mathbf{Q}^2/[(D_{\text{self}}\mathbf{Q}^2)^2+\omega^2],$$

and hence to Eq. (1). By analogy, a Gaussian form of the van Hove total correlation function leads to

$$S(\mathbf{Q},\omega) = D\mathbf{Q}^2/[(D\mathbf{Q}^2)^2+\omega^2],$$

with D the diffusion coefficient corresponding to the total correlation function.

To illustrate the difference between D_{self} and D, consider two individual atomistic diffusion events on a lattice: (a) the vacancy mechanism, in which the vacancy exchanges sites with an atom, and (b) the direct interchange of two atoms, that does not involve vacancies. Process (a) leads to time dependence of both $G(\mathbf{r},t)$ and $G_{\text{self}}(\mathbf{r},t)$, whereas process (b) results in a time dependence only of $G_{\text{self}}(\mathbf{r},t)$, not of $G(\mathbf{r},t)$. The diffusion coefficient D that is measured by co-

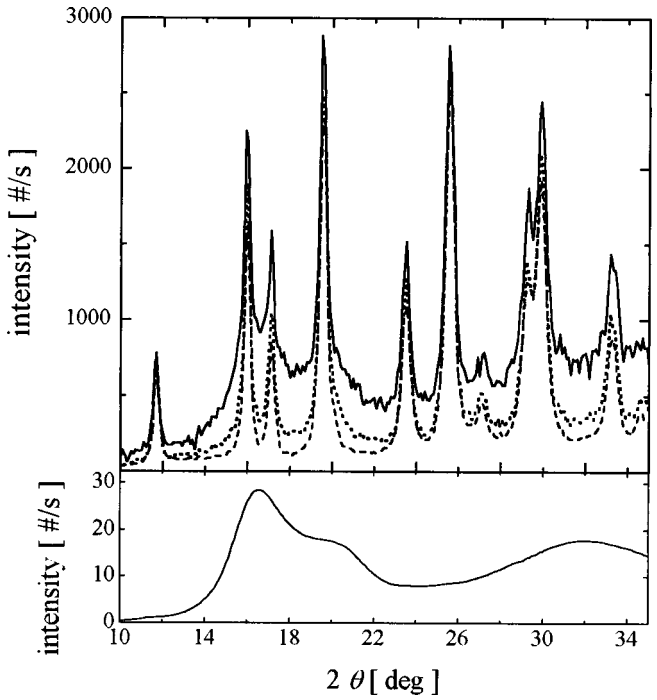

FIG. 1. Upper graph, x-ray diffraction pattern of pure nanocrystalline Al_2O_3 (dashed line), and two samples with $x=0.1$ Ga (dotted line) and $x=0.3$ Ga (solid line); lower graph, x-ray diffraction pattern of bulk liquid Ga at 320 K.

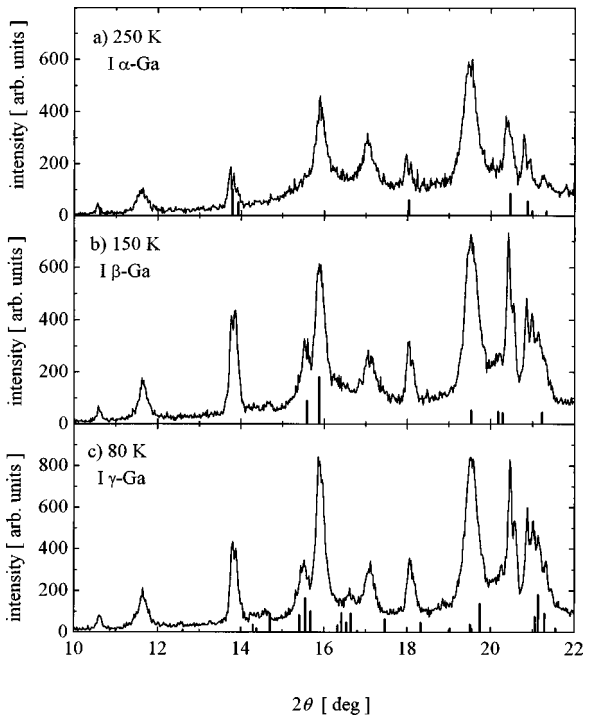

FIG. 2. Low-temperature x-ray diffraction pattern for a sample with $x=0.3$ Ga recorded at 250 K (a), 150 K (b), and 80 K (c). The solid lines are the theoretical Bragg positions of α-Ga (a), β-Ga (b), and γ-Ga (c).

herent QENS refers selectively to those atomic rearrangements that modify the local short-range order, such as (a). By contrast, rearrangements that maintain the local short-range order [such as (b)] do not contribute to D.

Assuming an energy transfer of 1 meV, we can calculate, by Eq. (1), that in this experiment diffusion coefficients in the range of 10^{-5} cm^2/s—a value typical for liquids—can easily be resolved. A further consequence of the coherent scattering is de Gennes narrowing,[23] that is, the diminishing of the observed half-width at wave vectors where the static structure factor $S(Q)$ has a maximum. Since for Ga this maximum in $S(Q)$ appears at 2.52 Å^{-1}, only the spectra recorded at Q values lower than 2 Å^{-1} have been analyzed in order to simplify the data evaluation process.

The neutron energy spectra recorded at different Q were grouped into ten summed spectra, with Q values in the range between 0.53 and 3.68 Å^{-1}, omitting the Bragg peaks of the crystalline Al_2O_3. These spectra were fitted by assuming a quasielastically broadened part due to diffusing Ga atoms with a mobile fraction q_{mobile} and an elastic contribution $(1-q_{\mathrm{mobile}})$ due to Ga atoms immobile at the time scale of this experiment. The data were analyzed by assuming Lorentzian line shapes, convoluted with an experimentally determined instrumental energy resolution function, for the quasielastically broadened line. To stabilize the fit a simultaneous data evaluation of six energy spectra for $Q<2$ Å^{-1} assuming that a Q^2 dependence of the half-width [Eq. (1)] was carried out for each temperature.

As discussed in Sec. III C below, a satisfactory fit to the energy spectra at each wave vector required the assumption of two superposed quasielastically broadened lines of different width. Altogether, each energy spectrum is therefore decomposed into three lines: one elastic line, with a profile exclusively due to the measured instrumental broadening, and two quasielastically broadened lines.

III. RESULTS

A. X-ray scattering

The upper graph in Fig. 1 depicts x-ray diffractograms for a pure nanocrystalline alumina sample and for as prepared samples with $x=0.1$ and 0.3 Ga, recorded at 293 K. All diffractograms show the Bragg reflections of α-alumina, but no additional peaks that might indicate crystalline Ga phases. From the broadening of the Bragg peaks the grain size of the alumina was determined to 25 ± 2 nm. At 293 K, the Ga-containing samples also show a background scaling in height with the Ga content. By comparison with the scattering of bulk liquid Ga (lower graph) the background is consistent with liquid or amorphous Ga.

Figure 2 shows the low-temperature x-ray-diffraction patterns for $x=0.3$, obtained upon cooling in the sequence 250, 150, and 80 K, together with literature data for the Bragg reflection positions of the α-, β-, and γ-Ga.[24–26] The grain size of the alumina phase was found to be invariant during cooling and reheating. Besides the alumina reflections, the patterns at and below 250 K showed reflections from crystalline α-Ga [Fig. 2(a)], at and below 150 K the β-Ga reflections are also present [Fig. 2(b)], and weak Bragg peaks of γ-Ga appear at 80 K [Fig. 2(c)]. Hence, during cooling α-Ga crystallizes between 293 and 250 K, β-Ga crystallizes between 250 and 150 K, and γ-Ga crystallizes between 150 and 80 K. Accordingly, the intensity of the amorphous back-

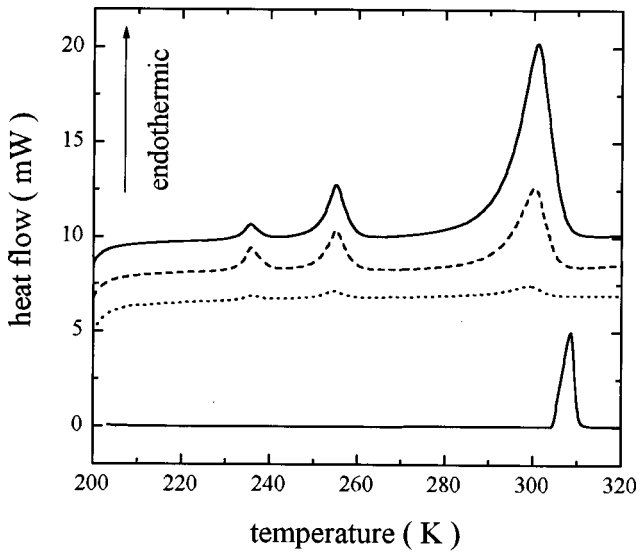

FIG. 3. DSC measurements for three samples with $x=0.2$ Ga (dotted line), $x=0.3$ Ga (dashed line), and $x=0.4$ Ga (upper solid line) and for a pure Ga reference sample (lower solid line).

ground is found to diminish with decreasing temperature. Due to the overlap of the Bragg reflections from the different crystalline phases the magnitude of the amorphous signal could not be quantified. However, the molar fractions of the individual phases can be determined from the calorimetric data.

B. Differential scanning calorimetry

In Fig. 3 the DSC measurements for three samples with $x=0.2$, 0.3, and 0.4 and for a pure bulk Ga reference sample is shown. The reference sample reveals a single endothermal peak with an onset temperature of 304.4 K, which agrees with the literature value of 302.93 K for a melting point of α-Ga.[7] The other samples show three broadened endothermal peaks with onset temperatures of 235, 250, and 290 K. These transitions are reversible, i.e., after cooling and reheating the peaks occurred again. The peaks can be related to the melting transitions of γ-, β-, and α-Ga: comparison with the corresponding melting temperatures from literature (237.55 K for γ-Ga and 256.85 K for β-Ga)[17] reveal a premelting by about 2 K for γ-Ga, 7 K for β-Ga and 13 K for α-Ga.

Figure 4 shows a heating and a subsequent cooling cycle for the sample with $x=0.3$. A comparison of the temperature intervals for melting and freezing reveals that in the case of the α-Ga the melting and freezing intervals overlap. Hence, α-Ga crystallizes without noticeable undercooling. For β-Ga the freezing is clearly shifted to lower temperatures. The freezing of γ-Ga was not detected by DSC. However, the low-temperature x-ray diffraction data recorded during cooling, show crystallization of γ-Ga between 150 and 80 K, well below the melting point of 237.55 K. Thus, both metastable phases (β- and γ-Ga) crystallize from the severely undercooled melt.

As indicated in Sec. II, we aim to estimate the molar faction of Ga that melts upon heating to 320 K, x_{molten}, from the molar enthalpies of fusion of the individual crystalline phases. The limited amount of melting point suppression justifies the use of literature data for the molar enthalpy of fusion in bulk for that purpose. Significant changes, relative to bulk, of the molar enthalpy of fusion in the crystallizing fraction, due to a potential effect of size or confinement, would result in corresponding variation of the melting points, and are thus ruled out by the data.

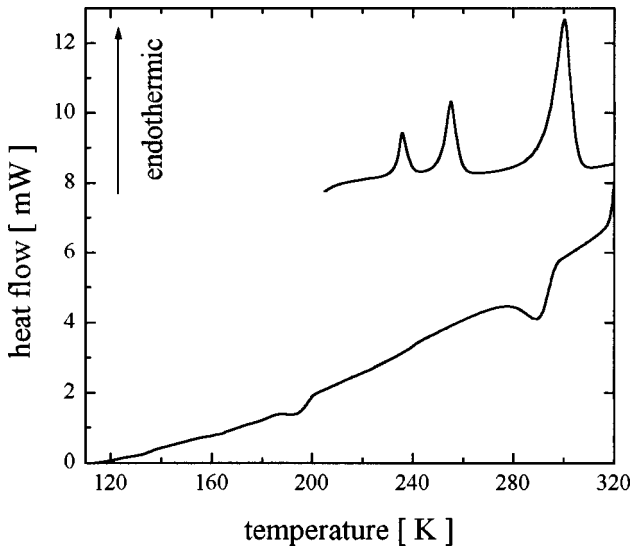

FIG. 4. Heating (upper line) and cooling (lower line) cycle for a sample with $x=0.3$ Ga.

Figure 5 shows the variation of x_{molten} with overall Ga molar fraction x, with x_{molten} determined as discussed above. By inspection of the figure, two ranges can be distinguished: in samples with $x<0.2$ only a small amount of Ga (1 mol %) can melt. For samples with $x\geqslant 0.2$, x_{molten} increases linearly with x. The dashed line was computed on the assumption that all Ga in excess of $x=0.18$ melts, and is seen to be in excellent agreement with the data. Thus, the finding is that up to a maximum molar fraction of 0.18, the Ga does not undergo a first-order phase transition in the temperature range 100–320 K, as suggested by the absence of measurable latent heat for that fraction.

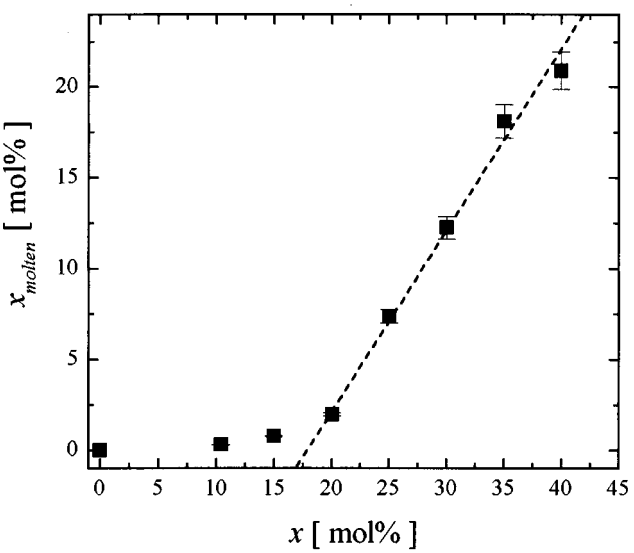

FIG. 5. Molar fraction of molten Ga x_{molten} for samples with different Ga contents. Explanation of the dashed line is in the text.

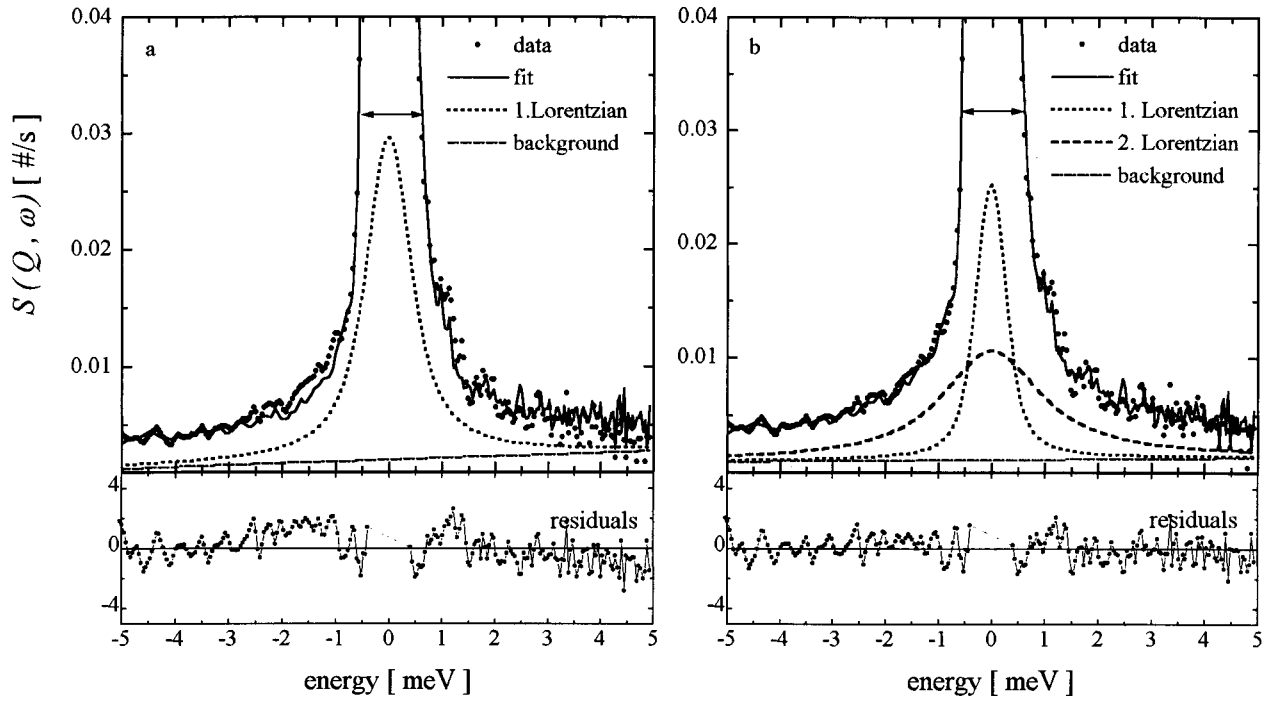

FIG. 6. Spectrum of scattered neutrons at $Q=0.82$ Å^{-1} and $T=320$ K (upper diagram) and corresponding residuals (lower diagram). (a) Fit with one Lorentzian, (b) fit with two Lorentzians.

C. Quasielastic neutron scattering

Figure 6 shows a typical quasielastic neutron scattering spectrum,[27] in the example $Q=0.82$ Å^{-1}, $T=320$ K. Beside an elastic contribution, one can clearly detect broadened wings due to quasielastic scattering of mobile Ga. By applying Eq. (1) to the elastic line of 506 μeV HWHM we deduce an upper limit of 10^{-6} cm^2/s for the diffusivity of the elastic component. Since this is much smaller than typical liquid diffusion coefficients, which are of the order of 10^{-5} cm^2/s, we shall refer to the matter that contributes to the elastic component as immobile, a notion that depends on the experimental energy resolution. Figures. 6(a) and 6(b) display the results of the fits with the elastic plus one or two quasielastically broadened lines, respectively. Systematic deviations between fit and experiment in the single-line cases, that are present at all temperatures, motivate the use of the two line fit, as detailed in Sec. II. The diffusion coefficients for different temperatures deduced by applying Eq. (1) to the two components are shown in Fig. 7. The lower diffusion coefficients agree within error bars with our finding for the bulk liquid Ga at 290 and 320 K. The faster diffusion coefficient is in the order of 10^{-4} cm^2/s.

Since in our QENS experiment, only the Ga contributes to the investigated spectra, the relative intensity of the quasielastically broadened line can be directly assigned to the amount of Ga that is mobile in terms of the experimental resolution, i.e., with diffusion coefficients larger than 10^{-6} cm^2/s. Thus we can compare the mobile Ga fraction q_{mobile} with the relative molar fraction of molten Ga deduced from the DSC data x_{molten}/x for the sample with $x=0.3$. Figure 8 displays the mobile Ga fraction q_{mobile} determined from the area under the broadened components in the quasielastic line, versus temperature (triangles and left ordinate) and the relative molar fraction of molten Ga x_{molten}/x that melts and crystallizes reversibly, and hence is molten at 320 K as determined by DSC (circles and right ordinate). For ease of reference, the DSC traces that illustrate the location of the melting transitions (compare with Fig. 3) are also depicted. It is seen that the endothermic DSC peaks which indicate melting transitions concur qualitatively with increases in the mobile fraction determined by QENS: At 250, 270, and 290 K, respectively, γ- and β- and part of the α-Ga

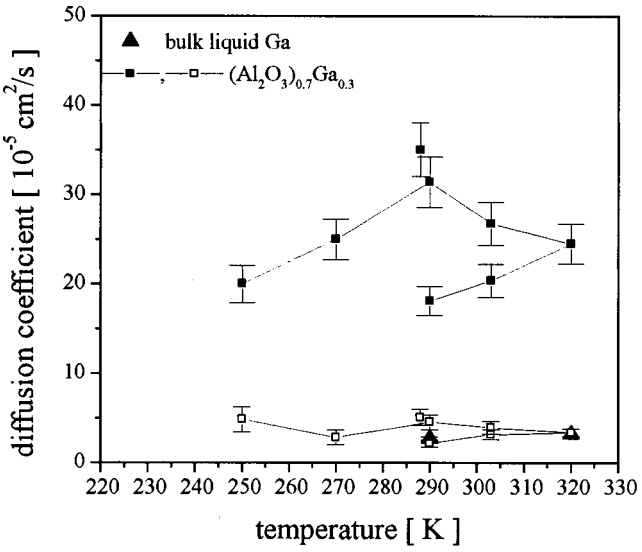

FIG. 7. Diffusion coefficients for a sample with $x=0.3$ (squares) and a bulk liquid Ga sample (triangles). The as-prepared sample was measured at 288 K, cooled to 77 K, and upon heating spectra at different temperatures up to 320 K were taken. Then, the measurements at 303 and 290 K were repeated upon cooling. The bulk liquid sample was measured at 320 K and in the undercooled liquid state at 290 K.

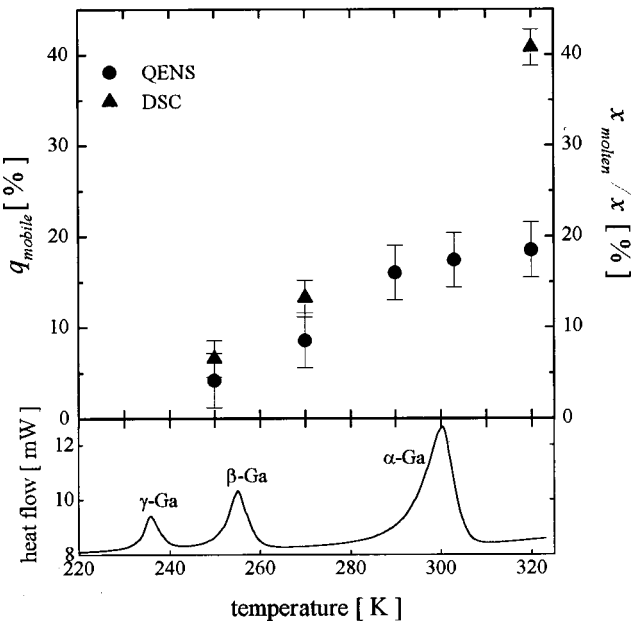

FIG. 8. Comparison of the mobile fraction q_{mobile} from QENS (left ordinate) with the relative molar fraction of molten Ga x_{molten}/x from DSC (right ordinate). The lower diagram shows the corresponding DSC measurement.

have melted and contribute to the quasielastic broadening. But at 303 and 320 K, where the α-Ga is completely molten, there is no quantitative agreement: the relative molar fraction of molten Ga inferred from the calorimetric data $x_{\mathrm{molten}}/x = 0.4$ is about twice the mobile fraction determined from the quasielastic neutron scattering $q_{\mathrm{mobile}} = 0.19$.

IV. DISCUSSION

Summarizing, the experimental results and the ensuing points of discussion are as follows: the Ga component is noncrystalline at 293 K, and upon cooling part of it crystallizes in a variety of stable and metastable phases. The total heat of fusion indicates that only a fraction of Ga actually crystallizes and melts upon cycling between 320 and 77 K; that fraction appears to be the Ga that is in excess of the molar fraction of 0.18. At least part of the molten Ga has a diffusivity that agrees within error bars with that of the bulk liquid. There is no evidence for a change of phase in the remaining Ga molar fraction of 0.18, and the QENS data imply that the diffusivity of that fraction is significantly below that of liquid Ga, even at temperatures up to 17 K above the bulk melting point. We shall first discuss why the metastable crystalline phases form and why they show undercooling, whereas the stable crystalline phase does not. Then, we proceed to discuss the nature of the remaining Ga.

The equilibrium phase of bulk Ga is the α-phase, but when undercooled to 256.7 K the Ga melt is known to crystallize in the metastable β phase, and upon further undercooling to 237.4 K the formation of yet another metastable phase, the γ-Ga, has been reported.[17] There are two reasons for undercooling to appear: for small particles it is often energetically favorable to remain liquid even below the bulk melting point because the surface energy of a liquid droplet is lower than the surface energy of the corresponding crystallite. Ga droplets are known to show this undercooling.[28] The second reason for undercooling is the presence of an energy barrier to build a solid nucleus and is also observed for bulk samples. Since the α-Ga does not show undercooling we can conclude that the nucleation barrier for the crystallization of α-Ga is insignificant. The β- and γ-Ga are present only to a small amount. From the observed undercooling of the β- and γ-Ga we can conclude that there is either a nucleation barrier for the freezing of these phases or that this part of the Ga could be present in the form of small droplets. Ga droplets are like to be formed due to the inhomogeneity of the preparation process. As has been pointed out above this would explain the formation of the metastable phases. The observed premelting of 2–13 K can be understood as an effect of reduced dimension or dimensionality. This phenomenon has often been observed for small particles[29] as well as for thin adsorbed films.[30]

The mobile fraction deduced from QENS increases with the fraction of molten Ga deduced from calorimetry for $T = 250$, 270, and 290 K. In addition, the measured diffusion coefficients agree with the value obtained for the bulk Ga reference sample at 290 and 320 K. This supports the conclusion that the formation of the metastable crystalline phases is through crystallization of droplets of bulk liquid.

The prominent properties of the remaining Ga are that $(1-q_{\mathrm{mobile}}) = 0.81$ of the Ga in the sample with $x = 0.3$, which corresponds to a molar fraction of 0.243 retains a diffusivity considerably below that of the bulk liquid throughout the investigated temperature range and hence up to 17 K above the bulk melting point. Furthermore, up to a molar fraction of 0.18 the Ga does not undergo a first order phase transition. As no bulk phase with those properties is known, we conjecture that the unusual behavior of this fraction of Ga results from an interfacial component, that is from layers of Ga confined at grain boundaries.

The thickness of the grain boundary film that accommodates a molar fraction of 0.243, the maximum molar fraction that shows reduced mobility, at the matrix grain size of 25 nm was computed to be equivalent to nine atomic monolayers in average. The molar fraction of 0.18, the maximum molar fraction that undergoes no first order phase transition, is equivalent to six atomic monolayers. These values are based on Eq. (3):[31]

$$Z = \frac{x \cdot \Omega_{\mathrm{Ga}}^{1/3} \cdot \mu}{(1-x) \cdot 3\Omega_{\mathrm{Al_2O_3}}}, \tag{3}$$

where Z denotes the number of monolayers, $\Omega = M_{\mathrm{mol}}/N_A \rho_{\mathrm{bulk}}$, M_{mol} the molar mass, N_A the Avogrado number, ρ_{bulk} the bulk density, and μ the surface mean diameter, which can be calculated from the mass mean diameter deduced from the broadening of the Bragg peaks. A similar behavior, i.e., nonmelting of Ga, has also been observed for the nanostructured WGa samples with a calculated interfacial layer thickness of five atomic monolayers.[32]

This observation is compatible with a model where the grain boundary film has outer layers, at each Al_2O_3-Ga interface, with a maximum thickness of three layers each, that do not melt and remain immobile above the bulk melting point and a core of thickness equivalent to three atomic monolayers, that undergo the structural phase transformation thus

contributing to the latent heat of fusion, but that retain low atomic mobility in the noncrystalline state for the most part (Fig. 8).

The phase transformation in the core layers, a transition between crystalline and noncrystalline state that involves latent heat of fusion, is evocative of the ''crystal to glass transition,'' a melting process induced by the shear instability of a crystalline alloy.[33] In both cases, the diffusion coefficient of the disordered phase is characteristic of a solid, the glass, as opposed to the liquid. But, in the present case, the transition in the core layers occurs near the bulk melting point and, hence, above the (bulk) glass transition temperature. This suggests that the confinement imposes severe restrictions on the kinetics of the core layer.

The observation, by calorimetry, that α-Ga crystallizes with negligible undercooling is also in agreement with the model: the outer layers provide sites for heterogeneous nucleation; alternatively, the phase transition may be continuous, proceeding progressively from the outer layers into the core when the temperature deviates from the transition onset. This effect has been observed experimentally in melting of intercalates.[5]

In terms of the model, the results of the QENS experiment indicates a diffusivity for the confined layers at the grain boundaries of less than 10^{-6} cm^2/s. Thus, the consistent observation of the absence of a melting transition and of low diffusivity for part of the Ga phase supports the idea that layerlike structures constrained between nanocrystallites may exhibit interesting properties in comparison to their bulk counterparts.

The slight increase in mobile fraction q_{mobile} at $T = 290$ K gives evidence of the partial contribution of the molten core to the quasielastically broadened line. The calculation of the layer thickness by Eq. (3) assumes a constant thickness of the layers. However, with the preparation method of ball milling we must, rather, assume an inhomogeneous distribution of Ga in the grain boundaries, thus the calculated thickness should be rather seen as an average value. Therefore, the core thickness may partially exceed the calculated average value of three layers and the liquid core may partially become mobile enough to have bulk liquid features, thus contributing to the quasielastic broadening.

The existence of a third diffusion coefficient, representative of kinetics faster than that of bulk liquid, remains puzzling. This fast diffusion coefficient may be due to surface diffusion on the external surface of the powder particles (as opposed to grains) produced by ball milling.

V. SUMMARY

We produced composites of nanocrystalline alumina and Ga. By using x-ray scattering, differential scanning calorimetry, and quasielastic neutron scattering, we could deduce the following structural model: The majority of the Ga is confined in the grain boundaries of the nanocrystalline alumina. About six layers of Ga are prevented from melting even 17 K above T_m^{Ga} due to the interaction with the confining matrix. If the sample contains more Ga, the average thickness of the grain boundary film increases. The excess Ga experiences a weaker interaction with the matrix and can melt. But there is strong indication that due to the confining geometric conditions the diffusion coefficient of these liquid layers is smaller than the diffusion coefficient of the bulk liquid. A small amount of Ga cannot be incorporated in the grain boundaries due to the inhomogeneity of the preparation process. This Ga is left over in the form of small droplets and freezes as β- and γ-Ga from the undercooled melt.

Presently further QENS experiments are planned. By choosing a better energy resolution we intend to measure smaller diffusion coefficients, i.e. the diffusion of the grain boundary film.

ACKNOWLEDGMENTS

This work was supported by the Sonderforschungsbereich 277 of the Deutsche Forschungsgemeinschaft and by the Human Capital Mobility Project of the European Community under Contract No. ERBCHRX-CT9-40433. The QENS measurements were supported by the Institut Laue Langevin, Grenoble. We wish to thank Jeremy Cook for technical assistance. We also thank Jörg Schmauch for his help with the DSC measurements.

*Present address: Shonan Institute of Technology, Tsujido Nishikaigan 1-1-25, Fujisawa 251, Japan.

[1] A. Bonnissent and B. Mutafshiev, Crit. Rev. Solid State Mater. Sci. **14**, 297 (1981).
[2] S. T. Chui, Phys. Rev. B **43**, 11 523 (1991).
[3] M. Schoen, D. J. Diestler, and J. H. Cushman, Phys. Rev. B **47**, 5603 (1993).
[4] E. Molz, A. P. Y. Wong, M. H. W. Chan, and J. R. Beamish, Phys. Rev. B **48**, 5741 (1993).
[5] H. Zabel, A. Magerl, J. J. Rush, and M. E. Misenheimer, Phys. Rev. B **40**, 7616 (1989).
[6] G. Devaud and R. H. Willens, Phys. Rev. Lett. **57**, 2683 (1986).
[7] M. Maruyama, M. Bienfait, J. G. Dash, and G. Codens, J. Cryst. Growth **118**, 33 (1992).
[8] J. Z. Larese, L. Passell, A. D. Heidemann, D. Richter, and J. P. Wicksted, Phys. Rev. Lett. **61**, 432 (1988).
[9] J. M. Gay and J. M. Kang, Physica B **180/181**, 474 (1992).
[10] D. M. Zhu and J. G. Dash, Phys. Rev. Lett. **57**, 2959 (1986).
[11] K. W. Herwig and F. R. Trouw, Phys. Rev. Lett. **69**, 89 (1992).
[12] J. Israelachvili, P. McGuiggan, M. Gee, A. Homola, M. Robbins, and P. Thompson, J. Phys.: Condens. Matter **2**, SA89 (1990).
[13] W. Krauss, Ph.D. thesis, Universitaet des Saarlandes, Saarbrücken, Germany, 1995.
[14] R. Birringer, H. Gleiter, H. P. Klein, and P. Marquardt, Phys. Lett. **102A**, 365 (1984).
[15] C. C. Koch, Mater. Sci. Forum **88-89**, 243 (1992).
[16] A. Kochendoerfer, Z. Kristallog. Mineral. u. Petrogr. **105**, 193 (1944).
[17] L. Bosio, A. Defrain, and I. Epelboin, J. Phys. (France) **27**, 61 (1966).
[18] M. Bee, *Quasielastic Neutron Scattering* (Hilger, London, 1988).
[19] *The Yellow Book, Guide to Neutron Research Facilities at the ILL*, edited by H. Blank and B. Maier (ILL, Grenoble, 1988).
[20] M. W. Johnson, UKAEA, Harwell, Berks., UK, Report No. AERE-R-7682, 1974 (unpublished).
[21] K. Skoeld and D. L. Price, in *Methods of Experimental Physics, Vol. 23, Neutron Scattering*, edited by R. Celotta and J. Levine, (Academic, San Diego, 1987).

[22] J. Philibert, *Atom Movements-Diffusion and Mass Transport in Solids* (Les Editions de Physique, Paris, 1991).
[23] P. G. de Gennes, Physica (Utrecht) **25**, 825 (1959).
[24] H. Swanson and R. Fuyat, NBS Circular **539**, 9 (1953).
[25] R. D. Heyding, W. Keeney, and S. L. Segel, J. Phys. Chem. Solids **34**, 133 (1973).
[26] Bosio *et al.*, J. Chim. Phys. **68**, 542 (1971).
[27] H. Konrad, C. Karmonik, J. Weissmueller, H. Gleiter, and R. Hempelmann, Physica B **234-236**, 173 (1997).
[28] D. Turnbull, Trans. AIME **188**, 1144 (1950).
[29] R. Kofmann, P. Cheyssac, and R. Garrigos, Phase Transit. **24-26**, 283 (1990).
[30] J. W. M. Frenken and H. M. van Pixteren, *The Chemical Physics of Solid Surfaces and Heterogeneous Catalysis*, edited by D. A. King (Elsevier, Amsterdam, 1994), Chap. 7.
[31] J. Weissmueller, Nanostruct. Mater. **3**, 261 (1992).
[32] W. Krauss (unpublished).
[33] M. Li and W. L. Johnson, Phys. Rev. Lett. **70.8**, 1120 (1993).